# Molecular-resolution imaging of lead phthalocyanine molecules by small amplitude frequency modulation atomic force microscopy using second flexural mode

Takashi Ichii,[1,a)] Yoshihiro Hosokawa,[1] Kei Kobayashi,[2] Kazumi Matsushige,[1] and Hirofumi Yamada[1,b)]

[1]*Department of Electronic Science and Engineering, Kyoto University, Katsura, Nishikyo, Kyoto 615-8510, Japan*

[2]*Innovative Collaboration Center, Kyoto University, Yoshida-Honmachi, Sakyo, Kyoto 606-8501, Japan*

(Received 7 December 2008; accepted 15 March 2009; published online 2 April 2009)

Lead phthalocyanine molecules on $MoS_2(0001)$ substrates were imaged using an ultrahigh-vacuum AFM apparatus equipped with an optical beam deflection (OBD) sensor. The second flexural mode was employed to utilize its high effective spring constant in order to reduce the oscillation amplitude to 0.5 nm without oscillation instability. Submolecular-resolution images were obtained when a shorter cantilever, which had a very high resonance frequency and a low noise equivalent deflection in the OBD sensor, was used. © *2009 American Institute of Physics*. [DOI: 10.1063/1.3114380]

Frequency modulation atomic force microscopy (FM-AFM), which is also known as noncontact atomic force microscopy, has been widely used to investigate various surfaces including insulating samples at atomic or molecular resolution.[1] In FM-AFM, the frequency shift in the force sensor is proportional to the integration of the interaction forces ($F_{ts}$) during an oscillation cycle with a weight function, which has one of the maxima at the closest point.[2] Several research groups have pointed out that the reduction in oscillation amplitude is significantly effective at obtaining high-resolution images because it leads to the selective detection of short-range chemical interaction forces.[3] However, the tip may jump into a static contact or the oscillation becomes unstable unless a force sensor with a high spring constant is used. In general, the restoring force of the force sensor $kA$, which is a product of the vibration amplitude ($A$) and spring constant ($k$), should be larger than $F_{ts}$; otherwise the tip could be pulled into the surface. In addition, the energy dissipation caused by the tip-sample interaction should be smaller than the kinetic energy that can be put into the cantilever per cycle $\pi kA^2/Q$, where $Q$ is the quality factor of the force sensor; otherwise the oscillation becomes unstable.[2] Because the stiffness of the cantilevers commonly used for FM-AFM is on the order of 10 N/m, the oscillation amplitude is typically larger than 5 nm.

Recently, Kawai *et al.*[4] reported high-resolution FM-AFM images on a Si(111)-7×7 surface with an oscillation amplitude of less than 0.1 nm by the use of the second flexural resonance mode, whose effective spring constant was about 40 times larger than that of the first resonance mode.[5] They used a heterodyne laser Doppler interferometer for deflection sensing, which detects velocity and thereby has a higher sensitivity for oscillation at a higher frequency. In this letter, we report molecular-resolution FM-AFM imaging on lead phthalocyanine (PbPc) molecules using the second flexural resonance mode with an AFM apparatus with an optical beam deflection (OBD) sensor, which is the most common deflection sensor for AFM.

Two types of highly doped Si cantilevers (Nanosensors: NCH and NCL) with nominal spring constant of 40 N/m were used. The first resonance frequencies ($f_1$) for NCH and NCL were about 300 and 170 kHz, respectively. Because the resonance frequency of the second flexural mode is 6.3 times as high as that of the first, the second resonance frequency ($f_2$) of NCH becomes about 1.9 MHz. A commercially available AFM apparatus (JEOL: JSPM-4500) was used with some modifications of the optics and the electronics in a similar way as described previously[6] to reduce the noise and expand the bandwidth of the OBD sensor. All the experiments were performed in an ultrahigh vacuum (UHV) environment whose base pressure was about $2\times10^{-8}$ Pa.

Figure 1 shows the frequency characteristics of the sensitivity of the OBD sensor measured by modulating the intensity of the laser. The red curve shows the amplitude of the modulated signal at the output of the current-to-voltage ($I$-$V$)

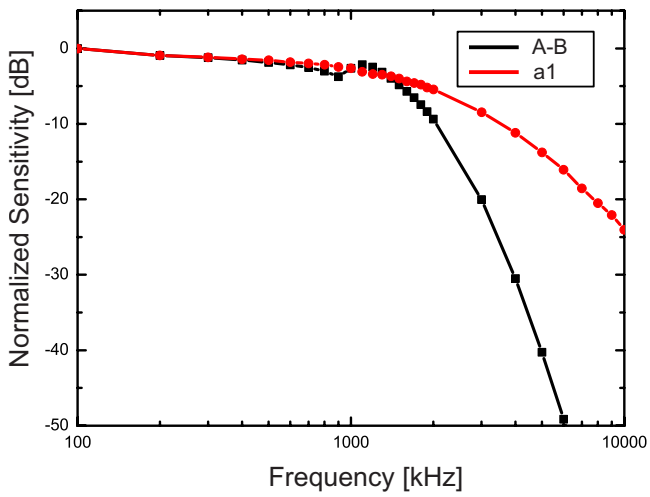


FIG. 1. (Color online) Frequency characteristics of the sensitivity of the OBD sensor: The red curve (a1) shows the normalized sensitivity of the photodiode and the preamplifier. The black curve (A-B) shows the normalized sensitivity of the OBD sensor including the differential amplifier.

[a)]Present address: Department of Materials Science and Engineering, Kyoto University, Yoshida-Honmachi, Sakyo, Kyoto 606-8501, Japan.
[b)]Electronic mail: h-yamada@kuee.kyoto-u.ac.jp.

 

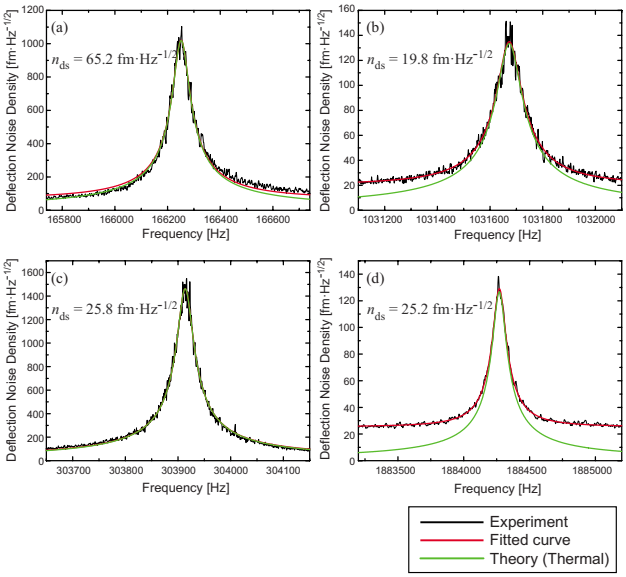


FIG. 2. (Color online) Thermal noise spectra of the cantilevers measured in UHV: (a) NCL at the first flexural resonance mode, (b) NCL at the second flexural resonance mode, (c) NCH at the first flexural resonance mode, and (d) NCH at the second flexural resonance mode. The black curves show experimentally measured spectra. The red lines show the fitted curves on the measured spectra. The green lines show the theoretical thermal noise spectra without deflection sensor noise.

converter connected to one segment of a segmented photodiode, normalized by the value for the modulation frequency of 100 kHz. The black curve shows the normalized signal amplitude at the output of the differential amplifier. Both curves show that the cutoff frequency, at which the signal attenuates from the value at 100 kHz by −3 dB of the OBD sensor, was about 1.3 MHz. The limiting factor of the bandwidth is the relatively large input capacitance of the *I-V* converter, which includes the junction capacitance of the photodiode and the coaxial cable connected to the *I-V* converter located outside the vacuum chamber.

Figures 2(a) and 2(b) show thermal noise spectra of the NCL cantilever around $f_1$ and $f_2$, respectively. The deflection noise density, corresponding to the noise equivalent deflection, was converted from the voltage density of the output signal of the OBD sensor by assuming a nominal spring constant. Because the square of the observed noise density ($n_{\mathrm{tot}}^2$) is the sum of the square of the deflection sensor noise ($n_{\mathrm{ds}}$) and the thermal noise ($n_{\mathrm{th}}$), $n_{\mathrm{ds}}$ is derived as $n_{\mathrm{ds}}=\sqrt{n_{\mathrm{tot}}^2-n_{\mathrm{th}}^2}$; $n_{\mathrm{ds}}$ was 65.2 fm/$\sqrt{\mathrm{Hz}}$ around $f_1$ and 19.8 fm/$\sqrt{\mathrm{Hz}}$ around $f_2$. It was found that $n_{\mathrm{ds}}$ at $f_2$ was about three times smaller than that at $f_1$. This is because the deflection noise density is inversely proportional to the sensitivity of the OBD sensor and the OBD sensor detects the angle of the location of the laser spot on the cantilever rather than the deflection itself. Thus, the deflection noise density of shorter cantilevers is generally smaller than that of longer ones. Since the effective cantilever length of the higher flexural mode is shorter than that of the fundamental mode, the deflection noise density of the higher flexural mode is also decreased as discussed in detail below. The cantilever displacement perpendicular to the cantilever axis at location $x$ is given by the equation

$$\nu_n(x) = A_n\left\{(\sin k_n x - \sinh k_n x) + \frac{\sin k_n L + \sinh k_n L}{\cos k_n L + \cosh k_n L}(\cosh k_n x - \cos k_n x)\right\}, \quad (1)$$

with the boundary condition $\cos k_n L \cosh k_n L + 1 = 0$. $A_n$ is a normalizing constant, $k_n$ is a mode-dependent constant, and $L$ is the cantilever length. It was easily obtained that the change in the angle at the cantilever end for a given displacement at $f_2$ was about 3.5 times larger than that at $f_1$.[5]

Figures 2(c) and 2(d) also show the thermal noise spectra of the NCH cantilever around $f_1$ and $f_2$, respectively. $n_{\mathrm{ds}}$ was 25.8 fm/$\sqrt{\mathrm{Hz}}$ around $f_1$ and 25.2 fm/$\sqrt{\mathrm{Hz}}$ around $f_2$. $n_{\mathrm{ds}}$ measured at $f_1$ of the NCH cantilever was lower than that measured at $f_1$ of the NCL cantilever. This was due to the difference in the cantilever length. The length of the NCH cantilever was typically 125 $\mu$m and that of the NCL cantilever was typically 225 $\mu$m. On the other hand, unlike in the case of the NCL cantilever, $n_{\mathrm{ds}}$ at $f_2$ of the NCH cantilever was 25.2 fm/$\sqrt{\mathrm{Hz}}$, which was almost same as that at $f_1$. This is because $f_2$ of the NCH cantilever was about 1.88 MHz, which was much higher than the cutoff frequency of the present OBD sensor. At a frequency range higher than the cutoff frequency, the sensitivity was decreased and the electronic noise was the dominant noise source, which remained almost constant. Therefore, the noise equivalent deflection was not decreased in this case. The minimum detectable force gradient ($F'_{\mathrm{min}}$) can be approximately calculated by the following equation on the assumption that the vibrating amplitude is small enough:

$$F'_{\mathrm{min}} = 2k\frac{\sqrt{\langle \delta f\rangle^2}}{f} = \sqrt{\frac{4kk_BTB}{\pi f Q A^2} + \frac{8k^2 n_{\mathrm{ds}}^2 B^3}{3f^2A^2}}, \quad (2)$$

where $\delta f$ is frequency noise, $k_{\mathrm{B}}$ is Boltzmann constant, $T$ is temperature, and $B$ is bandwidth.[7] Since $F'_{\mathrm{min}}$ for the second flexural mode of NCH calculated with the typical imaging parameters and the measured $n_{\mathrm{ds}}$ was smaller compared to NCL, NCH cantilevers were chosen for the imaging experiments.

We performed the second flexural FM-AFM imaging of PbPc ultrathin films on $MoS_2(0001)$ substrates. The molecules were deposited in a vacuum chamber connected to the AFM chamber. The samples were transferred *in situ* to the AFM sample stage. The NCH cantilever was self-oscillated at $f_2$ in a constant amplitude mode and its resonance frequency was detected with a home-built FM detector.[8] FM-AFM images were collected in the constant frequency shift mode. No bias voltage was applied between the tips and the samples.

Figure 3(a) shows a topographic image of a PbPc monolayer. The oscillation amplitude was about 0.8 nm. It can be seen clearly that individual molecules formed into square lattice structures with a period of 1.3 nm. In addition, a single molecular defect can be seen clearly in the lower left-hand corner (indicated by a black arrow), which means true molecular resolution imaging was achieved. Figure 3(b) shows an energy dissipation image obtained simultaneously with Fig. 3(a). This image also shows molecular-scale contrast and a single molecular defect (indicated by a white arrow).

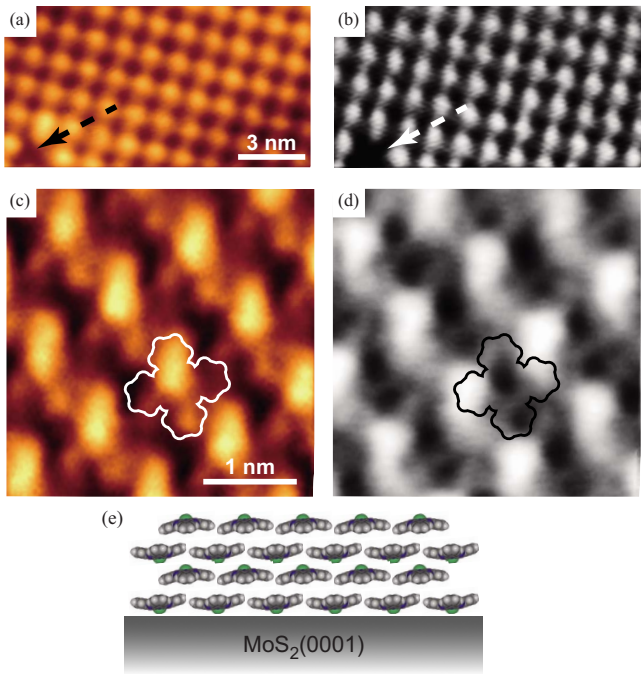


FIG. 3. (Color online) (a) Topographic FM-AFM image of a PbPc monolayer obtained using the second flexural mode. The scanned area was 13.7 $\times$7.3 nm$^2$. ($f_2$=1.861 796 MHz, $\Delta f$=−18 Hz, $A$=0.8 nm, and $Q_2$ =20 918.) (b) Energy dissipation image obtained simultaneously with (a). (c) Topographic image of a PbPc multilayer obtained using the second flexural mode. The scanned area was 4.1$\times$4.1 nm$^2$. ($f_2$=1.856 653 MHz, $\Delta f$ =−50 Hz, $A$=0.5 nm, and $Q_2$=22 369.) (d) Energy dissipation image obtained simultaneously with (c). (e) Schematic of the PbPc multilayer on the $MoS_2(0001)$ substrate.

Figures 3(c) and 3(d) show a topographic image of a PbPc multilayer (approximately four to six layers) and the corresponding energy dissipation image, respectively. The oscillation amplitude was about 0.5 nm. The topographic image showed submolecular-scale contrast with asymmetric four-leaf structures. One possible reason of the asymmetric structures is a slight tilt of the PbPc molecules, as schematically shown in Fig. 3(e). We cannot deny the possibility that this was due to a tip artifact. However, previous studies indicated that some metal phthalocyanines formed into monolayers or multilayers were not completely parallel to the substrates and slightly tilted.[9–11] Our result agreed well with those studies. The center of the PbPc molecules was higher than the surrounding region, which suggested that the PbPc molecules were directed upward. The energy dissipation image also showed submolecular-scale contrast. Although the origin of the energy dissipation contrast difference shown in Figs. 3(b) and 3(d) is not still clear, this could be because the structural properties are different between the monolayer film and the multilayer film.

The lateral resolution of the FM-AFM images taken here with the small amplitude FM-AFM was not greatly improved compared to that obtained with the conventional large amplitude FM-AFM.[10,11] One possible reason was because the vibrating amplitude in this experiment was still too large to detect the short-range interaction dominantly. Actually, the amplitude could not be decreased to less than 0.5 nm, which should be because the smallest amplitude was determined by the second criteria as mentioned above. Energy dissipation on molecules has a tendency to be larger than that on inorganic materials.[12] In addition, previous studies suggested that molecular fluctuation was induced by a tip-sample interaction, which would lead to the energy dissipation.[10,13] Considering these results, we can conclude that the reduction in the vibrating amplitude was limited by large energy dissipation on the PbPc molecules.

In summary, molecular-resolution imaging was performed using the second flexural resonance frequency with a modified commercial AFM apparatus operated in an UHV condition. Even though the bandwidth of the OBD sensor was limited to about 1.3 MHz, the oscillation amplitude at the second flexural resonance mode at 1.88 MHz was reduced to 0.5 nm with a sufficiently small noise equivalent deflection ($n_{ds}$: 25 fm/$\sqrt{\text{Hz}}$). PbPc ultrathin films were imaged with a submolecular resolution using this method.

This work was supported by a Grant-in-Aid for Scientific Research S (No. 19106001), a Grant-in-Aid for Research Fellowships, and Global COE Program from Japan Society for the Promotion of Science.

[1] *Noncontact Atomic Force Microscopy*, edited by S. Morita, R. Wiesendangaer, and E. Meyer (Springer, Berlin, Heiderblg, 2002), and references therein.
[2] F. J. Giessibl, S. Hambacher, H. Bielefeldt, and J. Mannhart, Science **289**, 422 (2000).
[3] F. J. Giessibl, H. Bielefeldt, S. Hambacher, and J. Mannhart, Appl. Surf. Sci. **140**, 352 (1999).
[4] S. Kawai, S. Kitamura, D. Kobayashi, S. Meguro, and H. Kawakatsu, Appl. Phys. Lett. **86**, 193107 (2005).
[5] S. Rast, C. Wattinger, U. Gysin, and E. Meyer, Rev. Sci. Instrum. **71**, 2772 (2000).
[6] T. Fukuma, M. Kimura, K. Kobayashi, K. Matsushige, and H. Yamada, Rev. Sci. Instrum. **76**, 053704 (2005).
[7] H. Yamada and K. Kobayashi, in *Applied Scanning Probe Methods VI*, edited by B. Bhushan and S. Kawata (Springer, Berlin, Heiderblg, 2006), Chap. 17.
[8] K. Kobayashi, H. Yamada, H. Itoh, T. Horiuchi, and K. Matsushige, Rev. Sci. Instrum. **72**, 4383 (2001).
[9] M. Takada and H. Tada, Chem. Phys. Lett. **392**, 265 (2004).
[10] T. Fukuma, K. Kobayashi, H. Yamada, and K. Matsushige, J. Appl. Phys. **95**, 4742 (2004).
[11] T. Yoda, T. Ichii, T. Fukuma, K. Kobayashi, H. Yamada, and K. Matsushige, Jpn. J. Appl. Phys., Part 1 **43**, 4691 (2004).
[12] L. Nony, P. Bennewitz, O. Pfeiffer, E. Gnecco, A. Baratoff, E. Meyer, T. Eguchi, A. Gourdon, and C. Joachim, Nanotechnology **15**, S91 (2004).
[13] M. Fendrich, T. Kunstmann, D. Paulkowski, and R. Möller, Nanotechnology **18**, 084004 (2007).